An efficient meshless method based on the Moving Kriging interpolation for two- dimensional variable-order time fractional mobile/immobile advection-diffusion model

Ali Habibirad, Esmail Hesameddini, Mohammad Hossein Heydari, Reza Roohi

1.Department of Mathematics, Shiraz University of Technology, Shiraz, Iran.

2.Department of Mechanical Engineering, Faculty of Engineering, Fasa University, Fasa, Iran

Abstract

In this work, we introduce an efficient meshless technique for solving the two-dimensional variable-order time-fractional mobile/immobile advection-diffusion model with Dirichlet boundary conditions. The main advantage of this scheme is to obtain a global approximation for this problem which reduces such problems to a system of algebraic equations. To approximate the first and fractional variable-order against the time, we use the finite difference relations. The proposed method is based on the Moving Kriging (MK) interpolation shape functions. To discretization this model in space variables, we use the MK interpolation. Duo to the fact that the shape functions of MK have Kronecker's delta property, boundary conditions are imposed directly and easily. To illustrate the capability of the proposed technique on regular and irregular domains, several examples are presented in different kinds of domains and with uniform and nonuniform nodes. Also, we use this scheme to simulating anomalous contaminant diffusion in underground reservoirs.

Keywords: Meshless local Petrov-Galerkin (MLPG) method, variable-order fractional derivative, Moving Kriging (MK) interpolation.
2000 MSC: 65M12,65M60, 34A45.

1. Introduction

In the past two decades, fractional calculus has demonstrated its capability in modeling unusual behaviors perceived in different kinds of engineering and science [1, 2, 3, 4]. So, their computations have been the focus of interest for many researchers. Therefore, applications and theory of fractional calculus quickly expanded [5, 6]. It is very difficult or impossible to find the analytical solution for fractional differential

equations (FDEs), thus numerical methods are mostly used to solve them. In recent years many different numerical methods have been applied for FDEs e.g. [7, 8, 9, 10, 8, 11] and references therein. We recall that the fractional partial differential equations (FPDEs) are extensions of classical partial differential equations (PDEs). Since the order of fractional derivatives and integrals can have any arbitrary values, various developments are considered in this concept. Unlike the classical fractional calculus, we consider the order of fractional derivatives/integrals be a known function of space and/or time variable(s). This is a generalization of classical fractional derivatives/integrals as variable-order (V-O) fractional derivatives/integrals [12, 13, 14].

V-O fractional calculus is suitable for developing the feature memory which varies with location or time. Applications of the V-O opinion have been expanded by many researchers, e.g. [15, 16, 17, 18, 19, 20].

Advection-dispersion equation and its generalization (e.g. the mobile/immobile equation) are a composition of advection and diffusion equations. These equations are applied to model many problems in chemicals, physical engineering, sciences of the earth [21], energy, transformation of contaminants, deeper river stream and groundwater [22, 23, 24, 25, 26].

Recently, mobile/immobile fractional differential equation has attracted attentions of many interested researchers. In this study, we consider the following fractional mobile/immobile advection-diffusion model in two dimensional as

$$\frac{\partial \Psi(\mathbf{x},t)}{\partial t} + \lambda_1 \frac{\partial^{\alpha(\mathbf{x},t)} \Psi(\mathbf{x},t)}{\partial t^{\alpha(\mathbf{x},t)}} = \lambda_2 \frac{\partial^2 \Psi(\mathbf{x},t)}{\partial x^2} + \lambda_3 \frac{\partial^2 \Psi(\mathbf{x},t)}{\partial y^2} + \lambda_4 \frac{\partial \Psi(\mathbf{x},t)}{\partial x} + \lambda_5 \frac{\partial \Psi(\mathbf{x},t)}{\partial y} + f(\mathbf{x},t), \quad (1.1)$$

subject to the initial and boundary conditions

$$\Psi(\mathbf{x},0) = g(\mathbf{x},t), \qquad \mathbf{x} = (x,y) \in \Omega \subset \mathbb{R}^2,$$
$$\Psi(\mathbf{x},t) = h(\mathbf{x},t), \quad \mathbf{x} \in \partial\Omega, t \in [0,T], \tag{1.2}$$

where $\frac{\partial^{\alpha(\mathbf{x},t)}}{\partial t^{\alpha(\mathbf{x},t)}}$ is the fractional differential operator with respect to t in the Caputo type as follows

$$\frac{\partial^{\alpha(\mathbf{x},t)} \Psi(\mathbf{x},t)}{\partial t^{\alpha(\mathbf{x},t)}} = \begin{cases} \frac{1}{\Gamma(1-\alpha(\mathbf{x},t))} \int_0^t \frac{1}{(t-\eta)^{\alpha(\mathbf{x},t)}} \frac{\partial \Psi(\mathbf{x},\eta)}{\partial \eta} d\eta, & 0 < \alpha(\mathbf{x},t) < 1, \\ \frac{\partial \Psi(\mathbf{x},t)}{\partial t}, & \alpha(\mathbf{x},t) = 1. \end{cases} \tag{1.3}$$

In Eq. (1.1) $\lambda_1, \lambda_2, \lambda_3, \lambda_4$ and λ_5 are known constants. Moreover, g, f and h are given functions. Many numerical methods have been used for solving fractional mobile/immobile equation in Multi-dimensional case. Authors of [27] proposed an implicit Euler scheme for this equation in one dimension. Salehi and co-authors used the discrete Hahn polynomials for the numerical solution of this equation in two dimensional [28]. Authors of [29] expanded a numerical simulation for this equation.

Meshfree techniques [30, 31, 32] are very interesting and impressive for solving PDEs since these methods include simple projecting, variety in solving metamorphosis and have capability to improve non-smooth solutions. The meshless local Petrov-Galerkin (MLPG) method is an efficient meshfree method to solve PDEs with complicated domains. Atluri [33] discussed six different kinds of MLPG techniques by changing the local weighting function which are called MLPG1, MLPG2,..., MLPG6. They are the localized asymmetric weak

form scheme (MLPG1), the collocation scheme (MLPG2), the discrete least-square method (MLPG3), the local boundary integration method (MLPG4), the local Heaviside asymmetric method (MLPG5) and the local Galerkin symmetric scheme (MLPG6) (for other properties see [34, 35, 36]). The major superiority of these methods compared to the other meshless schemes based on the weak form is the use of local weak form in each sub-domain (Ω_s) instead of a global weak form. Moving least square (MLS) is used to construct the shape functions of MLPG methods [33]. In the MLPG method based on MLS approximation, applying of essential boundary conditions is difficult, since the MLS shape functions don't have the Kronecker delta attribute. We use the moving Kriging (MK) interpolation instead of MLS approximation to create shape functions of the MLPG scheme. With this change, the MLPG shape functions have the Kronecker delta property. So, we can impose the Dirichlet boundary conditions directly and easily. Some authors have employed and improved the MLPG approach based on the MK interpolation [37, 38, 39]. Here, we use the MLPG2 method based on MK interpolation to obtain numerical solution of mobile/immobile (1.3).

The structure of this article is as follows: In Section 2, we briefly refer to the variable-order fractional calculus. In the next Section, the MK interpolation and its shape functions are brought. In Section 4, we introduce the MLPG2 based on MK interpolation to get the numerical solution of fractional mobile/immobile advection-diffusion model. To evaluate the accuracy and efficiency of the present method, several examples are given in Section 5 with various regular and irregular domains and distributed nodes. A momentous application of fractional calculus is simulation of pollution transport in the underground water reservoirs. We do this simulation in the last example. Finally, this article will be end with a conclusion.

2. The fractional calculus with variable-order (V-O)

In this part, we briefly refer to the variable order fractional calculus. Also, we provide some definitions which are needed in our work.

Definition 2.1. If $\beta > 0$, the one parameter Mittag-Leffler function is defined as follows [40]

$$E_\beta(w) = \sum_{i=0}^{\infty} \frac{w^i}{\Gamma(i\beta + 1)}, \qquad w \in \mathbb{R}.$$

Definition 2.2. If $\beta_1, \beta_2 > 0$, the two parameters Mittag-Leffler function is defined as follows [40]

$$E_{\beta_1, \beta_2}(w) = \sum_{i=0}^{\infty} \frac{w^i}{\Gamma(i\beta_1 + \beta_2)}, \qquad w \in \mathbb{R}.$$

REMARK 1. The following feature is an important issue in the V-O fractional definition

$$\frac{\partial^{\alpha(\mathbf{x},t)} t^n}{\partial t^{\alpha(\mathbf{x},t)}} = \frac{n!}{\Gamma(n + 1 - \alpha(\mathbf{x},t))} t^{n - \alpha(\mathbf{x},t)}, \quad n \in \mathbb{N}, \quad 0 < \alpha(\mathbf{x},t) \le 1.$$

3. The moving Kriging (MK) interpolation

The MK interpolation is a well-known geostatic technique for spatial interpolation in geology and mining [41, 42]. In the following, we will explain the building of meshless shape function by using MK interpolation.

Assume that the problem domain $\Omega \subseteq \mathbb{R}^2$ is discretized by a set of properly scattered nodes $\mathbf{x}_i$, $i = 1, 2, \ldots, n$ and $u(\mathbf{x})$ is a function defined in Ω. Similar to the MLS approximation, assume that only N nodes surrounding point $\mathbf{x}$ have the effect on $u(\mathbf{x})$. The MK interpolation $u^h(\mathbf{x})$ is defined as follows [41, 43]

$$u^h(\mathbf{x}) = \sum_{i=1}^{N} \phi_i(\mathbf{x}) u_i = \Phi(\mathbf{x}) \mathbf{u}, \quad \mathbf{x} \in \Omega_x, \tag{3.1}$$

where

$$\Phi(\mathbf{x}) = \mathbf{p}^T(\mathbf{x}) A + \mathbf{r}^T(\mathbf{x}) B. \tag{3.2}$$

Matrices A and B are known by the following equations:

$$A = (P^T R^{-1} P)^{-1} P^T R^{-1}, \tag{3.3}$$
$$B = R^{-1}(I - PA), \tag{3.4}$$

in which I is an $N \times N$ unit matrix and vector $\mathbf{p}(\mathbf{x})$ is

$$\mathbf{p}^T(\mathbf{x}) = [p_1(\mathbf{x}) \cdots p_m(\mathbf{x})], \tag{3.5}$$

where $p_j(\mathbf{x}), j = 1, 2, \ldots, m$ is the m polynomial basis functions, which have monomial terms. For example, for a two-dimensional problem, the linear basis is $\mathbf{p}^T(\mathbf{x}) = [1, x, y]$ and the quadratic basis is $\mathbf{p}^T(\mathbf{x}) = [1, x, y, x^2, y^2, xy]$. Note that we will use a linear basis in our computations in the next sections. Values of the polynomial basis functions (3.5) at the given set of nodes are collected in the matrix P as follows

$$P = \begin{bmatrix} p_1(\mathbf{x}_1) & \cdots & p_m(\mathbf{x}_1) \\ \cdots & \cdots & \cdots \\ p_1(\mathbf{x}_N) & \cdots & p_m(\mathbf{x}_N) \end{bmatrix}. \tag{3.6}$$

Also, the vector $\mathbf{r}(\mathbf{x})$ in (3.2) is given by

$$\mathbf{r}^T(\mathbf{x}) = \begin{bmatrix} \gamma(\mathbf{x}, \mathbf{x}_1) & \cdots & \gamma(\mathbf{x}, \mathbf{x}_N) \end{bmatrix}, \tag{3.7}$$

where $\gamma(\mathbf{x}, \mathbf{x}_j)$ is the correlation function between any pair of nodes located at $\mathbf{x}$ and $\mathbf{x}_j$. Many functions can be used as a correlation function. In this paper, we use the weight function as follows

$$\gamma(\mathbf{x}, \mathbf{x}_i) = \begin{cases} 1 - 6d_i^2 + 8d_i^3 - 3d_i^4, & d_i \leq 1, \\ 0, & d_i > 1, \end{cases} \tag{3.8}$$

where $d_i = \frac{\|\mathbf{x}-\mathbf{x}_i\|}{r_i}$, in which r_i is the size of support in weight function. In addition, the correlation matrix R is given in the following form :

$$R = \begin{bmatrix} \gamma(\mathbf{x}_1, \mathbf{x}_1) & \cdots & \gamma(\mathbf{x}_1, \mathbf{x}_N) \\ \cdots & \cdots & \cdots \\ \gamma(\mathbf{x}_N, \mathbf{x}_1) & \cdots & \gamma(\mathbf{x}_N, \mathbf{x}_N) \end{bmatrix}. \tag{3.9}$$

The first-order partial derivatives of shape function $\Phi(\mathbf{x})$ against the coordinates x and y can be easily obtained from (3.2) as

$$\frac{\partial \Phi(\mathbf{x})}{\partial x} = \frac{\partial \mathbf{p}^T(\mathbf{x})}{\partial x} A + \frac{\partial \mathbf{r}^T(\mathbf{x})}{\partial x} B, \tag{3.10}$$

$$\frac{\partial \Phi(\mathbf{x})}{\partial y} = \frac{\partial \mathbf{p}^T(\mathbf{x})}{\partial y} A + \frac{\partial \mathbf{r}^T(\mathbf{x})}{\partial y} B. \tag{3.11}$$

The shape function $\Phi(\mathbf{x})$ obtained by the MK interpolation possesses the delta function property. For the other properties of MK based on the shape functions see [41, 43, 42].

4. Numerical implementation

The local sub-domains overlap each other and cover the whole global domain Ω. They could be of any geometric shape and size [44]. Here, we use the collocation scheme (MLPG2) to obtain numerical solution of V-O time fractional advection-diffusion Eq. (5.2). So, the local weak form of (5.2) is as follows

$$\int_{\Omega_s} \left(\frac{\partial \Psi(\mathbf{x}, t)}{\partial t} + \lambda_1 \frac{\partial^{\alpha(\mathbf{x}, t)} \Psi(\mathbf{x}, t)}{\partial t^{\alpha(\mathbf{x}, t)}} \right) \nu \, d\Omega = \int_{\Omega_s} \left(\lambda_2 \frac{\partial^2 \Psi(\mathbf{x}, t)}{\partial x^2} + \lambda_3 \frac{\partial^2 \Psi(\mathbf{x}, t)}{\partial y^2} \right. \tag{4.1}$$
$$\left. + \lambda_4 \frac{\partial \Psi(\mathbf{x}, t)}{\partial x} + \lambda_5 \frac{\partial \Psi(\mathbf{x}, t)}{\partial y} + f(\mathbf{x}, t), \right) \nu \, d\Omega,$$

in which $\nu = \nu(\mathbf{x}, t)$ is the test function. We will use the collocation Dirac's Delta function $\delta(\mathbf{x} - \mathbf{x}_I)$ as the test function in each sub-domains Ω_s. So, the Eq. (4.1) is transferred to

$$\frac{\partial \Psi(\mathbf{x}_I, t)}{\partial t} + \lambda_1 \frac{\partial^{\alpha(\mathbf{x}_I, t)} \Psi(\mathbf{x}_I, t)}{\partial t^{\alpha(\mathbf{x}_I, t)}} = \lambda_2 \frac{\partial^2 \Psi(\mathbf{x}_I, t)}{\partial x^2} + \lambda_3 \frac{\partial^2 \Psi(\mathbf{x}_I, t)}{\partial y^2} + \lambda_4 \frac{\partial \Psi(\mathbf{x}_I, t)}{\partial x} + \lambda_5 \frac{\partial \Psi(\mathbf{x}_I, t)}{\partial y} + f(\mathbf{x}_I, t). \tag{4.2}$$

Assuming just N points in the neighborhood node $\mathbf{x}_k$ have the effect on the numerical solution. So, we have

$$\Psi^h(\mathbf{x}, t) = \sum_{j=1}^{N} \phi_j(\mathbf{x}) \hat{\Psi}_j(t). \tag{4.3}$$

Substituting the MK interpolation (4.3) in Eq. (4.2), the following system for all nodes will be obtained

$$\left(\frac{\partial \Psi^h(\mathbf{x}_I, t)}{\partial t} + \lambda_1 \frac{\partial^{\alpha(\mathbf{x}, t)} \Psi^h(\mathbf{x}_I, t)}{\partial t^{\alpha(\mathbf{x}, t)}} \right) C = K \Psi(\mathbf{x}_I, t) + F. \tag{4.4}$$

Note that C is an unit matrix because the shape functions obtained by the MK interpolation have the δ Kronecker property, and

$$K_{Ij} = \lambda_2 \frac{\partial^2 \phi_j(\mathbf{x}_I)}{\partial x^2} + \lambda_3 \frac{\partial^2 \phi_j(\mathbf{x}_I)}{\partial y^2} + \lambda_4 \frac{\partial \phi_j(\mathbf{x}_I)}{\partial x} + \lambda_5 \frac{\partial \phi_j(\mathbf{x}_I)}{\partial y}, \qquad F_I = f(\mathbf{x}_I, t).$$

To generate a fully discrete scheme of Eq .(4.4), let $\tau = \frac{T}{n}$ be the step size of time. So, we define $t_k = k\tau, k = 0, 1, 2, \ldots, n$, where n is a positive integer. To approximate V-O fractional derivative, we use the following finite difference technique [45]

$$\frac{\partial^{\alpha(\mathbf{x},t)} \Psi(\mathbf{x}, t_{n+1})}{\partial t^{\alpha(\mathbf{x},t)}} = a(\mathbf{x}, t_{n+1}) \left[\Psi_{n+1} - \Psi_n + \sum_{k=1}^{n} b_k(\mathbf{x}, t_{n+1}) \left(\Psi_{n-k+1} - \Psi_{n-k} \right) \right] + O\left(\tau^{2-\alpha(\mathbf{x},t_{n+1})} \right), \quad (4.5)$$

where $a(\mathbf{x}, t_{n+1}) = \frac{\tau^{-\alpha(\mathbf{x},t_{n+1})}}{\Gamma(2-\alpha(\mathbf{x},t_{n+1}))}, b_k(\mathbf{x}, t_{n+1}) = (k+1)^{1-\alpha(\mathbf{x},t_{n+1})} - (k)^{1-\alpha(\mathbf{x},t_{n+1})}$ and $\Psi_n = \Psi(\mathbf{x}, n\tau)$. Also,

$$\frac{\partial \Psi(\mathbf{x}_I, t)}{\partial t} = \frac{\Psi_{n+1} - \Psi_n}{\tau}, \qquad \Psi = \frac{1}{2}(\Psi_{n+1} + \Psi_n). \tag{4.6}$$

Substituting (4.5) and (4.6) in (4.4), results in

$$\left[(1 - \lambda_1 a_{n+1}\tau) C - \frac{\tau}{2}K \right] \Psi_{n+1} = \left[(1 + \lambda_1 a_{n+1}\tau) C + \frac{\tau}{2}K \right] \Psi_n \tag{4.7}$$

$$- \lambda_1 a_{n+1}\tau C \sum_{k=1}^{n} b_k(\mathbf{x}, t_{n+1}) \left(\Psi_{n-k+1} - \Psi_{n-k} \right) + \tau F_{n+1},$$

where $a_{n+1} = a(\mathbf{x}, t_{n+1})$ and $F_{n+1} = F(\mathbf{x}, t_{n+1})$.

5. Numerical examples

In this section, some test problems are given to indicate the efficiently and accuracy of the presented numerical scheme. Note that we suppose the global data density of X in Ω as follows [46]

$$h = h_{\Omega, X} = \sup_{\mathbf{x} \in \Omega} \min_{\mathbf{x}_i \in X} \|\mathbf{x} - \mathbf{x}_i\|.$$

Also, we use the cubic polynomial basis for constructing the MK interpolation shape functions. In all examples we illustrate the L_∞ error which is defined as follows

$$L_\infty = \max \|\Psi^{\text{Numerical}} - \Psi^{\text{Exact}}\|_\infty = \max_i \|\Psi_i^{\text{Numerical}} - \Psi_i^{\text{Exact}}\|,$$

in which $\Psi^{\text{Numerical}}$ and Ψ^{Exact} are numerical and exact solutions, respectively. Moreover, to evaluate the capability of our method, we report its order in time variable as

$$C - \text{order} = \frac{\log\left(\frac{L_\infty(\tau_1)}{L_\infty(\tau_2)} \right)}{\log\left(\frac{\tau_1}{\tau_2} \right)},$$

Table 1: The L_∞ errors and the $C-$order of present method for Example 1 over Ω_1 with $T = 1$.

τ	$\alpha = 0.5$	$C-$order	$\alpha = 0.7$	$C-$order	$\alpha(\mathbf{x}, t)$	$C-$order
0.001	$4.4962e-06$	$-$	$3.1261e-05$	$-$	$3.5573e-05$	$-$
0.001/2	$2.4215e-06$	0.8928	$1.5063e-05$	1.0534	$1.7157e-05$	1.0505
0.001/4	$1.2700e-06$	0.9311	$7.3031e-06$	1.0444	$8.3209e-06$	1.0440
0.001/8	$6.5548e-07$	0.9542	$3.5592e-06$	1.0370	$4.0646e-06$	1.0338

where, $L_\infty(\tau_1)$ and $L_\infty(\tau_2)$ are L_∞ error related to τ_1 and τ_2, respectively. These examples are investigated on the following domains

$$\Omega_i = \left\{(x, y) \in \mathbb{R}^2 : 0 \le x \le 1, 0 \le y \le 1\right\}, i = 1, 2, \qquad \text{(Rectangular)},$$

$$\Omega_i = \left\{(x, y) \in \mathbb{R}^2 : x = r_i \cos(\theta), y = r_i \sin(\theta), \ \theta \in [0, 2\pi]\right\}, i = 3, 4, 5, 6, \quad \text{(Polar)},$$

where $r_3 = r_4 = \frac{3}{4}\sqrt{\cos(5\theta) + \cos^2(2\theta) + \cos^2(\theta)}$ and $r_5 = r_6 = \frac{3}{256}(81 - 9\cos(8\theta))$. Nodal points distribution on $\Omega_i, i = 1, \ldots, 6$ are indicated in Fig. 1. In the case of irregular nodes, we use the Halton nodes.

EXAMPLE 1. Consider the following time V-O fractional mobile-immobile advection-dispersion model:

$$\frac{\partial \Psi(\mathbf{x}, t)}{\partial t} + \frac{\partial^{\alpha(\mathbf{x}, t)} \Psi(\mathbf{x}, t)}{\partial t^{\alpha(\mathbf{x}, t)}} = \frac{\partial^2 \Psi(\mathbf{x}, t)}{\partial x^2} + \frac{\partial^2 \Psi(\mathbf{x}, t)}{\partial y^2} - \frac{\partial \Psi(\mathbf{x}, t)}{\partial x} - \frac{\partial \Psi(\mathbf{x}, t)}{\partial y} + f(\mathbf{x}, t),$$

in which

$$f(\mathbf{x}, t) = 2t + \frac{2t^{2-\alpha(\mathbf{x}, t)}}{\Gamma(3 - \alpha(\mathbf{x}, t))} + 2x + 2y - 4.$$

The exact solution is $\Psi(\mathbf{x}, t) = x^2 + y^2 + t^2$. We have solved this example on Ω_1 and Ω_2. The initial and Dirichlet boundary conditions will be obtained by the exact solution. Three cases for $\alpha(\mathbf{x}, t)$ are chose as $\alpha(\mathbf{x}, t) = 0.5, 0.7$ and $\alpha(\mathbf{x}, t) = 0.8 - 0.1\cos(xt)\sin(x) - 0.1\cos(yt)\sin(y)$. This example is considered by the proposed method for $t \in [0, 1]$ and error between the exact and numerical solutions are shown in Tables 1 and 2.

Table 1 shows the L_∞ errors for different values of fractional order $\alpha(\mathbf{x}, t)$. Also, it shows the convergence order in time variable which computations are done in 21×21 uniform nodes (Ω_1).This table indicates that the proposed method has good accuracy for solving this example for uniform points .

Table 2 reveals the results obtained by the presented scheme in global domain Ω_2 (see Fig. 1). The number of irregular nodes in this case is 484. From this table, we councud that our method is capable for solving this problem in irregular distributed nodes. By comparison tables 1 and 2, one can see that this method in regular case is more accurate than irregular case.

Graphs of numerical results obtained for this example in final time $T = 1$ on global domain Ω_1 are depicted in Fig. 2, with $\tau = 0.001$. This figure illustrates that the obtained results are in a good agreement with the analytical solution.
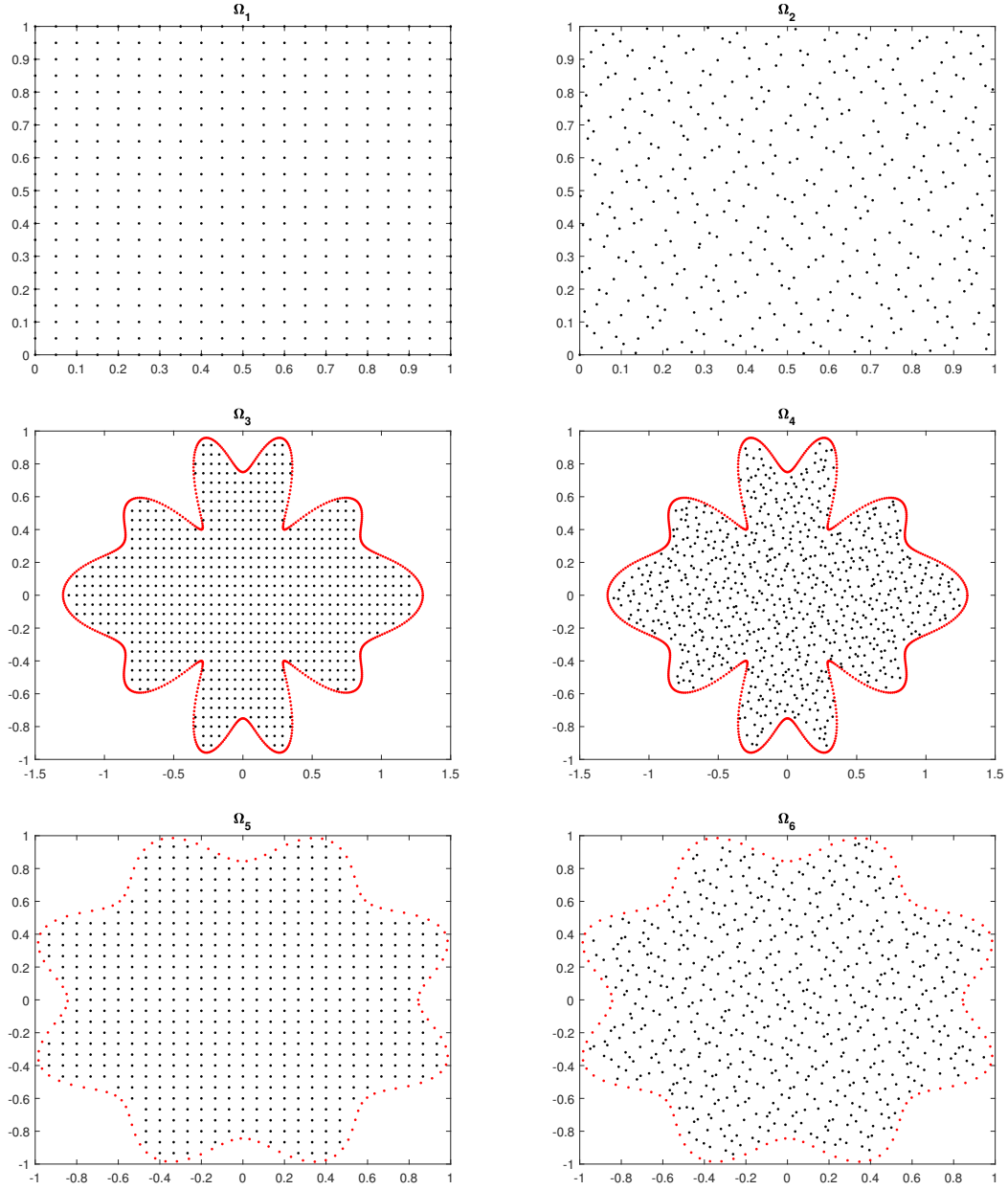
Fig. 1: Regular and irregular distributed nodes on the domains $\Omega_i, i = 1, 2, \ldots, 6$.

Table 2: The L_∞ errors and $C-$order of the presented method for Example 1 in Ω_2 with $T=1$.

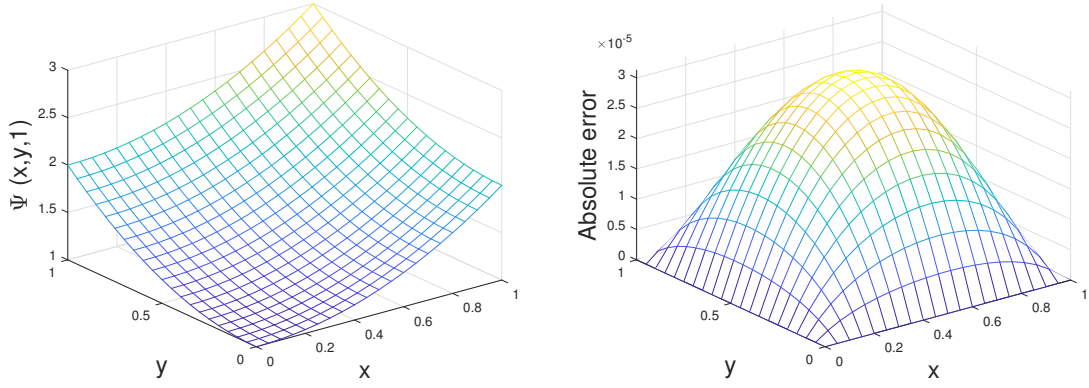| τ	$\alpha = 0.5$	$C-$order	$\alpha = 0.7$	$C-$order	$\alpha(\mathbf{x},t)$	$C-$order
0.001	$6.3748e-05$	$-$	$2.1764e-04$	$-$	$2.3062e-04$	$-$
0.001/2	$3.0911e-05$	1.0443	$1.0566e-04$	1.0425	$1.1199e-04$	1.0421
0.001/4	$1.5121e-05$	1.0316	$5.1539e-05$	1.0357	$5.4625e-05$	1.0357
0.001/8	$7.4434e-06$	1.0225	$2.5246e-05$	1.0296	$2.6749e-05$	1.0301

Fig. 2: Graphs of the numerical results for Example 1 at $t=1$ with $\tau = 0.001$ over Ω_1.

Table 3: The L_∞ errors and $C-$ order of presented method for Example 2 over Ω_3

τ	$\alpha = 0.5$	$C-$ order	$\alpha = 0.7$	$C-$ order	$\alpha(\mathbf{x},t)$	$C-$ order
0.001	$1.0683e-04$	$-$	$9.3108e-05$	$-$	$8.8223e-05$	$-$
0.001/2	$5.1198e-05$	1.0612	$4.4102e-05$	1.0781	$4.1289e-05$	1.0954
0.001/4	$2.3582e-05$	1.1184	$2.0006e-05$	1.1404	$1.8453e-05$	1.1619
0.001/8	$1.0266e-05$	1.1998	$9.3341e-06$	1.0998	$8.9519e-06$	1.0436

Table 4: The L_∞ errors and $C-$ order of the presented method for Example 2 over Ω_4 with $T = 2$.

τ	$\alpha = 0.5$	$C-$ order	$\alpha = 0.7$	$C-$ order	$\alpha(\mathbf{x},t)$	$C-$ order
0.01	$5.1201e-04$	$-$	$6.8332e-04$	$-$	$8.4566e-04$	$-$
0.01/2	$2.4241e-04$	1.0787	$3.2289e-04$	1.0815	$4.0135e-04$	1.0752
0.01/4	$1.1174e-04$	1.1173	$1.4941e-04$	1.1118	$1.8695e-04$	1.1022
0.01/8	$5.0408e-05$	1.1484	$6.6163e-05$	1.1752	$8.3222e-05$	1.1674

Results of tables 1,2 and Fig. 2 show that the proposed method has good accuracy for solving this example with regular and irregular distributed nodes.

EXAMPLE 2. In this example, we consider time variable fractional order mobile-immobile advection-dispersion model

$$\frac{\partial \Psi(\mathbf{x},t)}{\partial t} + \frac{\partial^{\alpha(\mathbf{x},t)} \Psi(\mathbf{x},t)}{\partial t^{\alpha(\mathbf{x},t)}} = \frac{\partial^2 \Psi(\mathbf{x},t)}{\partial x^2} + \frac{\partial^2 \Psi(\mathbf{x},t)}{\partial y^2} - \frac{\partial \Psi(\mathbf{x},t)}{\partial x} - \frac{\partial \Psi(\mathbf{x},t)}{\partial y} + f(\mathbf{x},t), \qquad (5.1)$$

where, $f(\mathbf{x},t) = \left[\cos(t) + t^{1-\alpha(\mathbf{x},t)} E_{2,2-\alpha(\mathbf{x},t)}(-t^2) - 4\sin(t)\right] e^{-(x+y)}$. The exact solution is $\Psi(\mathbf{x},t) = \sin(t)e^{-(x+y)}$. The boundary conditions are chosen Dirichlet, and will be determined from the exact solution. Also, the initial condition is $\Psi(\mathbf{x},t) = 0$. The results of numerical scheme for this example are obtained on global domains Ω_3 and Ω_4 (see Fig. 1).

Table 3 shows the computational on Ω_3 whit the regular distributed nodes. Here we use 629 nodes in boundary of Ω_3 and 765 uniform nodes in Ω_3. Also, we report the convergence order in time variable for different kinds of fraction variable order $\alpha(\mathbf{x},t)$. These results reveal that the proposed numerical scheme has good efficiency for solving this example and the convergence order in time variable is almost $O(\tau)$. The final time is $T = 1$ and the results are obtain for different time steps. The results of this table confirm that by decreasing the time step the L_∞ error is decreased.

In Table 4, the results of this problem by our method are compared with the analytical solution. Final time is $T = 2$ and the global domain is Ω_4. The number of nodes in boundary of Ω_4 is 629 and 765 irregular nodes are selected in interior domain Ω_4. The L_∞ errors related to different time steps are reported in this
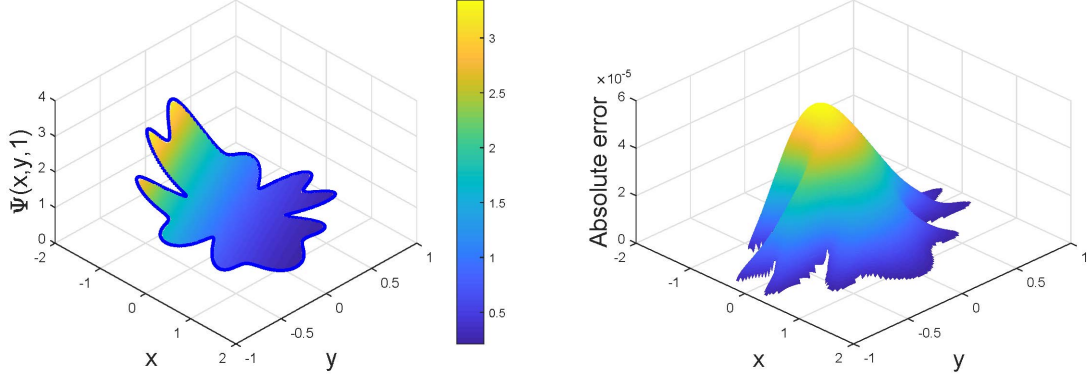
Fig. 3: Graphs of numerical solution and absolute error for Example 1 in $T = 1$ with $\tau = 0.001$ on Ω_3.

table. Also, the order of convergence are shown for different values of $\alpha(\mathbf{x}, t)$. From this table, we deduce that the our numerical scheme has nearly $O(\tau)$ order in time variable and has a good performance for solving this example in irregular distributed nodes. Also, this method is very efficient in large values of time for solving this example.

The absolute error between proposed scheme and analytical solution and behavior of approximation solution for this problem are plotted in Fig. 3. This figure illustrates that, the proposed method has good agreement with the exact solution for this example.

Tables 3, 4 and Fig. 3 reveal that our method is suitable and accurate to obtain numerical solution of this problem.

EXAMPLE 3. In this example, we consider the time variable fractional order mobile-immobile advection-dispersion model (1.1) in the following form

$$\frac{\partial \Psi(\mathbf{x}, t)}{\partial t} + \frac{\partial^{\alpha(\mathbf{x}, t)} \Psi(\mathbf{x}, t)}{\partial t^{\alpha(\mathbf{x}, t)}} = \frac{\partial^2 \Psi(\mathbf{x}, t)}{\partial x^2} + \frac{\partial^2 \Psi(\mathbf{x}, t)}{\partial y^2} - \frac{\partial \Psi(\mathbf{x}, t)}{\partial x} - \frac{\partial \Psi(\mathbf{x}, t)}{\partial y} + f(\mathbf{x}, t), \tag{5.2}$$

in which $f(\mathbf{x}, t) = \left[-e^{-t} + t^{\alpha(\mathbf{x}, t)} E_{1, 2-\alpha(\mathbf{x}, t)}(-t) + 2e^{-t}\right] \sin(x) \cos(y) + e^{-t} \cos(x) \cos(y) - e^{-t} \sin(x) \sin(y)$. The exact solution is $\Psi(\mathbf{x}, t) = \exp(-t) \sin(x) \cos(y)$. Similar to the previous examples, the Dirichlet boundary and initial conditions will be obtained from the exact solution. We solve this example by the presented method and the results will be compared with the exact solution. The L_∞ errors between our computations and the exact solution are reported in tables 5 and 6.

In Table 5, the results of our scheme are shown in different time steps. Here, the final time is $T = 1$ and global domain is Ω_5 (see Fig. 1). Also, we use 126 points on boundary of Ω_5 and 609 uniform nodes in interior. The constant values of fractional order $\alpha(\mathbf{x}, t)$ are $0.5, 0.7$ and the variable order is supposed to be $\alpha(\mathbf{x}, t) = 0.8 - 0.1 \cos(xt) \sin(x) - 0.1 \cos(yt) \sin(y)$. The L_∞ errors for these values are reported in the

11

Table 5: The L_∞ errors and the $C-$order of present method for Example 3 in Ω_5.

τ	$\alpha = 0.5$	$C-$order	$\alpha = 0.7$	$C-$order	$\alpha(\mathbf{x}, t)$	$C-$order
0.001	$3.6492e-05$	–	$3.8810e-05$	–	$4.0684e-05$	–
0.001/2	$1.7439e-05$	1.0653	$1.8609e-05$	1.0604	$1.9539e-05$	1.0581
0.001/4	$7.9149e-06$	1.1397	$8.5073e-06$	1.1292	$9.0119e-06$	1.1165
0.001/8	$3.2035e-06$	1.3049	$3.5397e-06$	1.2651	$3.7974e-06$	1.2468

Table 6: The L_∞ errors and $C-$order of presented method for Example 3 in Ω_6 with final time $T = 2$.

τ	$\alpha = 0.5$	$C-$order	$\alpha = 0.7$	$C-$order	$\alpha(\mathbf{x}, t)$	$C-$order
0.01	$1.5498e-04$	–	$1.6410e-04$	–	$1.5442e-04$	–
0.01/2	$7.7173e-05$	1.0059	$8.2121e-05$	0.9987	$7.7065e-04$	1.0027
0.01/4	$3.8628e-05$	0.9986	$4.1394e-05$	0.9883	$3.8582e-05$	0.9986
0.01/8	$1.9615e-05$	0.9777	$2.1204e-05$	0.9651	$1.9607e-05$	0.9766

second, forth and sixth columns of this table. Moreover, the third, fifth and seventh columns of this table demonstrate the $C-$order convergence in time variable for these values. From this table, we conclude that our method has a good accuracy and capability in regular nodes and almost $O(\tau)$ order in time variable.

Table 6 provides the numerical results for this example on global domain Ω_6 (see Fig. 1). These computational are done by using 126 nodes on the boundary of this domain, and 609 irregular nodes in its interior. Here the final time is $T = 2$ and the time steps decreased from $\tau = 0.01$ to $\tau = 0.01/8$ to get the $C-$order convergence in time variable. The different values of $\alpha(\mathbf{x}, t)$ are $0.5, 0.7$ and the variable order is considered as $\alpha(\mathbf{x}, t) = 1 - \exp(-xyt)$. The L_∞ errors related to this values are reported in columns $2, 4$ and 6 of this table, respectively. Also, the $c-$order for these values are given in columns $3, 5$ and 6, respectively. From this table we conclude that our method has a good efficiency in the large final time and irregular nodes with approximately $O(\tau)$ order in the time variable.

The graphs of the numerical solution and absolute error function at final time $T = 1$ with time steps $\tau = 0.001$ on global domain Ω_5 are depicted in Fig. 4. From this figure, one can see that our scheme has good performance for solving Example 3.

The results of tables 5, 6 and Fig. 4 reveal the accuracy and capability of the proposed scheme in the regular and irregular distributed nodes for solving this problem.

EXAMPLE 4. **Anomalous contaminant diffusion in underground reservoir**

One of the important applications of the examined fractional equation is the simulation of pollution transport in underground water reservoir. To be more specific, as the water passes across various underground soil layers, the natural or human-produced contaminants can penetrate into the main flow stream and pollute
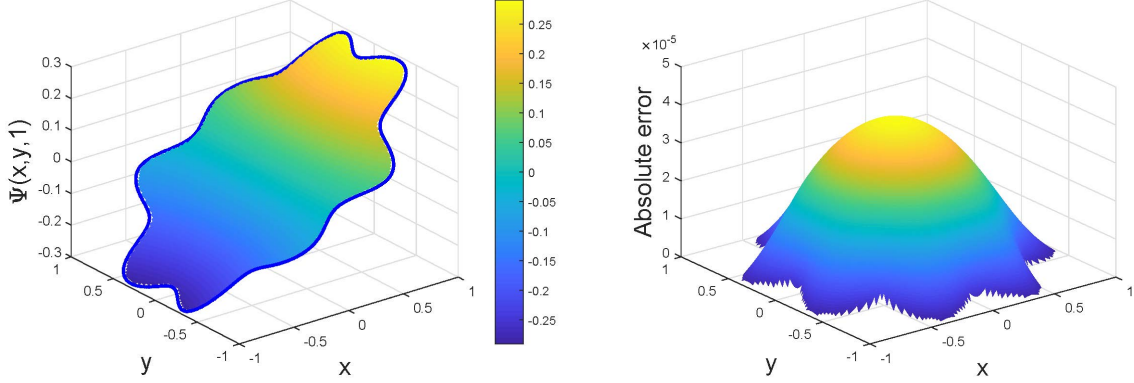
Fig. 4: Graphs of numerical solution and absolute error for Example 3 in $t = 1$ with $\tau = 0.001$ on Ω_5.

the flow entirely. Moreover, as the soil domain includes several heterogeneous pores, the conventional diffusion equation can not be applied and the incorporation of the anomalous diffusion is essential. In the present example, the transportation of the contaminant within a rectangular channel is numerically examined. To generalize the obtained results, it is assumed that the pollution can penetrate the flow stream due to the blowing/suction at the peripheral channel sides as well as generation inside the channel. Moreover, for the simulation of the pollutants advection through the channel the streamwise velocity profile is obtained and applied from the solution of the laminar steady Navier Stokes equation. Besides, a first order chemical reaction for pollutants removal is also accounted.

The pollution concentration governing equation as well as the initial and boundary conditions are represented in Eqs (5.3)-(5.5) as [47]

$$
\frac{\partial^\zeta \Psi(\mathbf{x}, t)}{\partial t^\zeta} + \mu^{1-\zeta} \left(\frac{W^2}{D}\right)^\zeta \frac{Re\vartheta}{W^2} \left[u(y)\frac{\partial \Psi(\mathbf{x}, t)}{\partial x} + v(y)\frac{\partial \Psi(\mathbf{x}, t)}{\partial y}\right] = \left(\frac{W^2}{\mu D}\right)^{\zeta-1} \left[\frac{\partial^2 \Psi(\mathbf{x}, t)}{\partial x^2} + \frac{\partial^2 \Psi(\mathbf{x}, t)}{\partial y^2}\right]
$$

$$
- K(\mathbf{x})\mu^{1-\zeta} \left(\frac{W^2}{D}\right)^\zeta \Psi(\mathbf{x}, t) + \mu^{1-\zeta}S(\mathbf{x}), \tag{5.3}
$$

where ζ, Ψ, W, K and D are the time fractional order, the pollution concentration, width of the channel, reaction rate coefficient and diffusion coefficient, respectively. Moreover, it should be noted that the variables in Eq. (5.3), as stated before, are dimensionless [48]. To account for the contaminant advection, the velocity components of u and v along and perpendicular to the flow stream are assumed, respectively. Additionally, μ is the time fractional constant, Re is the Reynolds number, ϑ is the kinematic viscosity and S represents

13

the pollution generation source. Eq. (5.3) is numerically solved with the following boundary conditions

$$\Psi(0, y, t) = 0, \qquad \frac{\partial \Psi(L/W, y, t)}{\partial x} = 0, \qquad (5.4)$$

$$\Psi(x, 0, t) = 0, \qquad \Psi(x, 1, t) = 0,$$

and with initial condition:

$$\Psi(x, y, t) = 0. \qquad (5.5)$$

According to the boundary conditions, it is assumed that a pollution free stream is entered the rectangular field from left, while the pollution concentration at the upper and lower faces are set to one and zero, respectively. Besides, the gradient free (fully developed) boundary condition at the channel outlet as well as zero concentration at the initial instance are also applied for physical modeling. As stated before, the velocity components are determined based on the solution of the laminar Navier-Stokes equation as

$$u(y) = \frac{-4}{Re\nu_0} \left(\frac{e^{\nu_0 y Re} - 1}{e^{\nu_0 Re} - 1} - y \right), \qquad (5.6)$$

$$v(y) = \nu_0. \qquad (5.7)$$

The pollution generation source is also assumed to be applied between locations of $x = a$ and $x = b$ as:

$$S(\mathbf{x}) = \frac{m}{1 + e^{-n(x-a)}} - \frac{m}{1 + e^{-n(x-b)}}, \qquad (5.8)$$

The constants in Eq. (5.8) are assigned as $m = 2000, n = 20, a = 1.0$ and $b = 1.5$. Based on the introduced governing equations, the proposed meshless scheme is applied and the results are represented in the following. The simulation is conducted with the following values for the affecting parameters: $\nu_0 = 0.2, \zeta = 0.7, Re = 20, K = 50, D = 10, W = 1.0$ and $L = 7.0$.

The contours of the variations of pollutant concentration within the simulated channel at the final time (Fig. 5-a) as well as the effect of fractional order magnitude on the concentration profile along a vertical line (Fig. 5-b) are revealed in Fig. 1. The vertical line is selected at $x = \frac{a+b}{2}$ which is the center of the pollution generation region. According to the concentration contours at the final time, it is observed that the boundary conditions at the peripheral channel surfaces are fully satisfied and the effect of pollution generation between $x = 1.0$ and $x = 1.5$ as a local accumulation of concentration is occurred. Additionally, regarding the effect of fractional order, it is shown that for lower magnitudes of the fractional order, the non-dimensional diffusion coefficient is intensified and leads to more propagation of the generated pollution. On the other hand, by increasing the fractional order the accumulation of contaminant in the source region grows significantly due to the lower diffusivity coefficient.

6. Conclusion

In the presented work, we applied a meshless scheme for solving V-O fractional mobile/immobile advection-diffusion equation. In this scheme we used the moving Kriging interpolation to contraction the shape functions
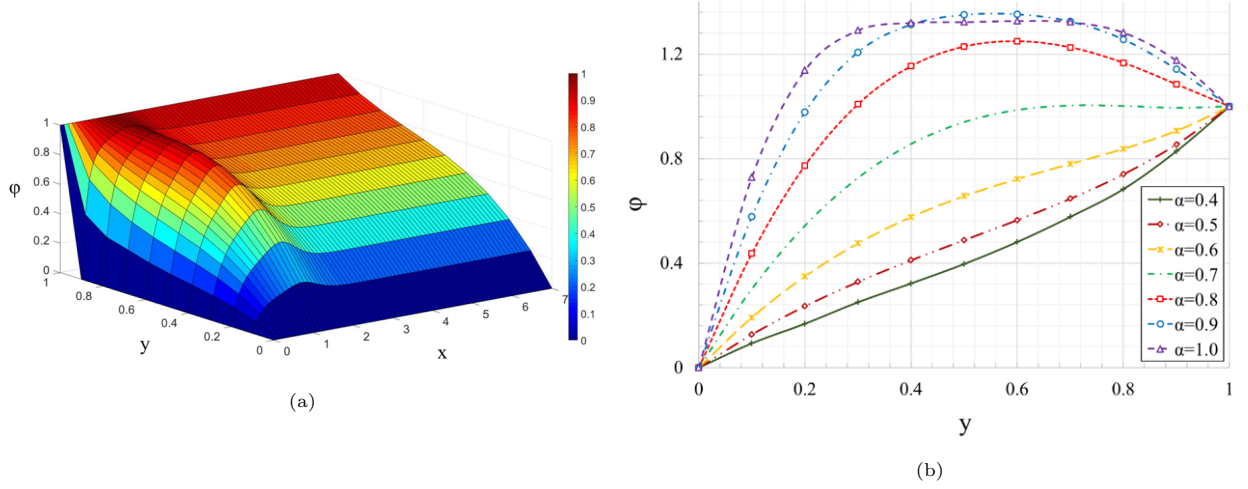
Fig. 5: The variations of the pollution concentration: a) contours at the final time and b) the effect of fractional order.

of MLPG2. By using this method, the boundary conditions were applied directly and easily. The Dirac's Delta was employed as a test function over the local sub-domains. To approximate the variable-order fractional derivative, we used the finite difference method. We investigated the capability and accuracy of the method by solving several examples. Also, we used this method to simulation pollution transport in underground water reservoirs. The obtained results showed that presented scheme was efficient with a good accuracy to handle these kinds of problems.

References

[1] Dumitru Baleanu, Kai Diethelm, Enrico Scalas, and Juan J Trujillo. Fractional calculus, vol. 3 of series on complexity, nonlinearity and chaos, 2012.

[2] Mark M Meerschaert and Charles Tadjeran. Finite difference approximations for fractional advection–dispersion flow equations. *Journal of Computational and Applied Mathematics*, 172(1):65–77, 2004.

[3] Keith Oldham and Jerome Spanier. *The fractional calculus theory and applications of differentiation and integration to arbitrary order*, volume 111. Elsevier, 1974.

[4] Igor Podlubny. Fractional differential equations, vol. 198 of mathematics in science and engineering, 1999.

[5] Xiao-Li Ding and Juan J Nieto. Analytical solutions for coupling fractional partial differential equations with dirichlet boundary conditions. *Communications in Nonlinear Science and Numerical Simulation*, 52:165–176, 2017.

[6] Song Wei, Wen Chen, and YC Hon. Characterizing time dependent anomalous diffusion process: A survey on fractional derivative and nonlinear models. *Physica A: Statistical Mechanics and its Applications*, 462:1244–1251, 2016.

[7] Weiping Bu, Yifa Tang, Yingchuan Wu, and Jiye Yang. Finite difference/finite element method for two-dimensional space and time fractional bloch–torrey equations. *Journal of Computational Physics*, 293:264–279, 2015.

[8] MH Heydari, Mohammad Reza Hooshmandasl, and FM Maalek Ghaini. An efficient computational method for solving fractional biharmonic equation. *Computers & Mathematics with Applications*, 68(3):269–287, 2014.

[9] MH Heydari, Mohammad Reza Hooshmandasl, FM Maalek Ghaini, and Carlo Cattani. Wavelets method for solving fractional optimal control problems. *Applied Mathematics and Computation*, 286:139–154, 2016.

[10] M Hosseininia, MH Heydari, R Roohi, and Z Avazzadeh. A computational wavelet method for variable-order fractional model of dual phase lag bioheat equation. *Journal of Computational Physics*, 2019.

[11] MH Heydari, MR Hooshmandasl, F Mohammadi, and C Cattani. Wavelets method for solving systems of nonlinear singular fractional volterra integro-differential equations. *Communications in Nonlinear Science and Numerical Simulation*, 19(1):37–48, 2014.

[12] Stefan G Samko and Bertram Ross. Integration and differentiation to a variable fractional order. *Integral transforms and special functions*, 1(4):277–300, 1993.

[13] Stefan G Samko. Fractional integration and differentiation of variable order. *Analysis Mathematica*, 21(3):213–236, 1995.

[14] Stefan Samko. Fractional integration and differentiation of variable order: an overview. *Nonlinear Dynamics*, 71(4):653–662, 2013.

[15] Carl F Lorenzo and Tom T Hartley. Initialization, conceptualization, and application in the generalized (fractional) calculus. *Critical Reviews^{TM} in Biomedical Engineering*, 35(6), 2007.

[16] D Ingman and J Suzdalnitsky. Control of damping oscillations by fractional differential operator with time-dependent order. *Computer Methods in Applied Mechanics and Engineering*, 193(52):5585–5595, 2004.

[17] J Orosco and CFM3545595 Coimbra. On the control and stability of variable-order mechanical systems. *Nonlinear Dynamics*, 86(1):695–710, 2016.

[18] Qiang Yu, Viktor Vegh, Fawang Liu, and Ian Turner. A variable order fractional differential-based texture enhancement algorithm with application in medical imaging. *PloS one*, 10(7):e0132952, 2015.

[19] GRJ Cooper and DR Cowan. Filtering using variable order vertical derivatives. *Computers & Geosciences*, 30(5):455–459, 2004.

[20] Abolhassan Razminia, Ahmad Feyz Dizaji, and Vahid Johari Majd. Solution existence for non-autonomous variable-order fractional differential equations. *Mathematical and Computer Modelling*, 55(3-4):1106–1117, 2012.

[21] Mark M Meerschaert, David A Benson, and Boris Bäumer. Multidimensional advection and fractional dispersion. *Physical Review E*, 59(5):5026, 1999.

[22] David A Benson, Rina Schumer, Mark M Meerschaert, and Stephen W Wheatcraft. Fractional dispersion, lévy motion, and the made tracer tests. *Transport in porous media*, 42(1-2):211–240, 2001.

[23] Zhiqiang Deng, Lars Bengtsson, and Vijay P Singh. Parameter estimation for fractional dispersion model for rivers. *Environmental Fluid Mechanics*, 6(5):451–475, 2006.

[24] Asma Ali Elbeleze, Adem Kilicman, and Bachok M Taib. Application of homotopy perturbation and variational iteration methods for fredholm integrodifferential equation of fractional order. In *Abstract and Applied Analysis*, volume 2012. Hindawi, 2012.

[25] Hossain Jafari, Abdelouhab Kadem, Dumitru Baleanu, and Tuğba Yılmaz. Solutions of the fractional davey-stewartson equations with variational iteration method. 2012.

[26] Sangdan Kim and M Levent Kavvas. Generalized fick's law and fractional ade for pollution transport in a river: Detailed derivation. *Journal of Hydrologic Engineering*, 11(1):80–83, 2006.

[27] H Zhang, Fawang Liu, Mantha S Phanikumar, and Mark M Meerschaert. A novel numerical method for the time variable fractional order mobile–immobile advection–dispersion model. *Computers & Mathematics with Applications*, 66(5):693–701, 2013.

[28] Farideh Salehi, Habibollah Saeedi, and Mahmood Mohseni Moghadam. A hahn computational operational method for variable order fractional mobile–immobile advection–dispersion equation. *Mathematical Sciences*, 12(2):91–101, 2018.

[29] MA Abdelkawy, MA Zaky, AH Bhrawy, and D Baleanu. Numerical simulation of time variable fractional order mobile-immobile advection-dispersion model. *Rom. Rep. Phys*, 67(3):773–791, 2015.

[30] Mehdi Dehghan and Ali Shokri. Numerical solution of the nonlinear klein–gordon equation using radial basis functions. *Journal of Computational and Applied Mathematics*, 230(2):400–410, 2009.

[31] Mehdi Dehghan and Ahmad Nikpour. Numerical solution of the system of second-order boundary value problems using the local radial basis functions based differential quadrature collocation method. *Applied Mathematical Modelling*, 37(18-19):8578–8599, 2013.

[32] Ali Shokri and Ali Habibirad. A moving kriging-based mlpg method for nonlinear klein–gordon equation. *Mathematical Methods in the Applied Sciences*, 39(18):5381–5394, 2016.

[33] Satya N Atluri and S Shen. *The meshless method.* Tech Science Press Encino, CA, 2002.

[34] Mehdi Dehghan and Rezvan Salehi. A meshless local petrov–galerkin method for the time-dependent maxwell equations. *Journal of Computational and Applied Mathematics*, 268:93–110, 2014.

[35] Mehdi Dehghan and Davoud Mirzaei. Meshless local petrov–galerkin (mlpg) method for the unsteady magnetohydrodynamic (mhd) flow through pipe with arbitrary wall conductivity. *Applied Numerical Mathematics*, 59(5):1043–1058, 2009.

[36] J Sladek, P Stanak, ZD Han, V Sladek, and SN Atluri. Applications of the mlpg method in engineering & sciences: a review. *CMES: Computer Modeling in Engineering & Sciences*, 92(5):423–475, 2013.

[37] Lei Gu. Moving kriging interpolation and element-free galerkin method. *International journal for numerical methods in engineering*, 56(1):1–11, 2003.

[38] P Phaochoo, A Luadsong, and N Aschariyaphotha. The meshless local petrov–galerkin based on moving kriging interpolation for solving fractional black–scholes model. *Journal of King Saud University-Science*, 28(1):111–117, 2016.

[39] Tinh Quoc Bui, Minh Ngoc Nguyen, and Chuanzeng Zhang. A moving kriging interpolation-based element-free galerkin method for structural dynamic analysis. *Computer Methods in Applied Mechanics and Engineering*, 200(13-16):1354–1366, 2011.

[40] Akira Hasegawa. Optical solitons in fibers. In *Optical Solitons in Fibers.* Berlin: Springer, 1989.

[41] L. Chen and K.M. Liew. J a local petrov-galerkin approach with moving kriging interpolation for solving transient heat conduction problems. *Comput. Mech.*, 47:455–467, 2011.

[42] L. Gu. Moving kriging interpolation and element-free galerkin method. *Int. J Numer. Meth. Eng*, 56:1–11, 2003.

[43] Q.Liang B. Dai, B. Zheng and L. Wang. Numerical solution of transient heat conduction problems using improved meshless local petrov-galerkin method. *Appl. Math. Comput*, 219:10044–10052, 2013.

[44] Satya N Atluri and Tulong Zhu. A new meshless local petrov-galerkin (mlpg) approach in computational mechanics. *Computational mechanics*, 22(2):117–127, 1998.

[45] Younes Shekari, Ali Tayebi, and Mohammad Hossein Heydari. A meshfree approach for solving 2d variable-order fractional nonlinear diffusion-wave equation. *Computer Methods in Applied Mechanics and Engineering*, 350:154–168, 2019.

[46] Fasshauer Gregory E. Meshfree approximation methods with matlab, usa world scientific (2007).

[47] Heydari M. H. Roohi R and Sun H. G. Numerical study of unsteady natural convection of variable-order fractional jeffrey nanofluid over an oscillating plate in a porous medium involved with magnetic, chemical and heat absorption effects using chebyshev cardinal functions. *The European Physical Journal Plus*, 134(10):535, 2019.

[48] Bavi O Roohi R, Heydari M. H and Emdad H. Chebyshev polynomials for generalized couette flow of fractional jeffrey nanofluid subjected to several thermochemical effects. *Engineering with Computers*, pages 1–17, 2019.